Supplementary Material

1 MULTIPLE OPTICAL CHANNELS ADDRESSING THE SAME TASK IN PARALLEL

Here, we present additional results regarding Section 4.2 of the main text. In this section, the system addresses multiple instances of the NARMA-10 task simultaneously. As described in detail in the main text, the simulation of the WDM MRR-based TDRC is done for a $\overline{P}_{\mathrm{T}}$ range of $[-20, 25]$ dBm, distributed equally over the channels, and a $\Delta\omega/2\pi$ range of $[-100, 100]$ GHz. The length of the datasets for training and testing is 2000 data points. First, we simulate the system for equal instances of the same task. In this case, as demonstrated in Fig. 3 of the main text, the system achieves an equal and excellent performance in all channels. In this case, the inter-coupling of the channels due to the free carrier dynamics benefits the performance of the system. Furthermore, in Fig. S1, we present the relative difference $|\Delta|$ between the performance of channel 0 and the rest of the channels over the parameter space of $\overline{P}_{\mathrm{i}}$ and $\Delta\omega_i$. We observe that $|\Delta|$ remains very low over the entirety of the parameter space. Then, we obtain the results for different instances of the same task (different sets of seeds) and obtain the results of Fig. S2. Here, as the data modulating each channel is different, the system does not benefit from the inter-coupling between the channels. We see a decrease in the performance of each channel and the minimum NMSE also becomes different from channel to channel (Fig. 4 in the main text). Consequently, the behavior of $|\Delta|$ varies between channels 0-1, channels 0-2, and channels 0-3. For example, the minimum $|\Delta|$ between channels 0 and 1 becomes significantly larger than the one between channels 0 and 3. As discussed in Section 4.7, this is likely also a consequence of the wavelength-dependent impact of the phase shift on each channel.

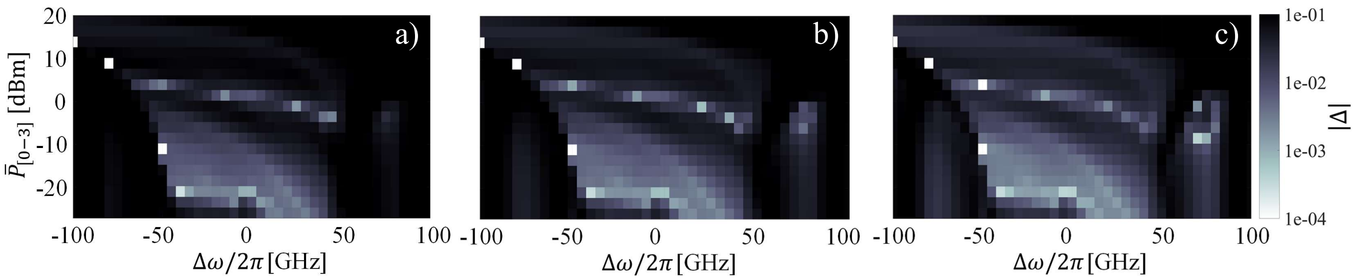

Figure S1. Difference in NMSE between: a) Channels 0 and 1, b) Channels 0 and 2, c) Channels 0 and 3, as a function of $\overline{P}_{\mathrm{i}}$ and $\Delta\omega_i/2\pi$ when addressing four equal instances of the NARMA-10 task in parallel.

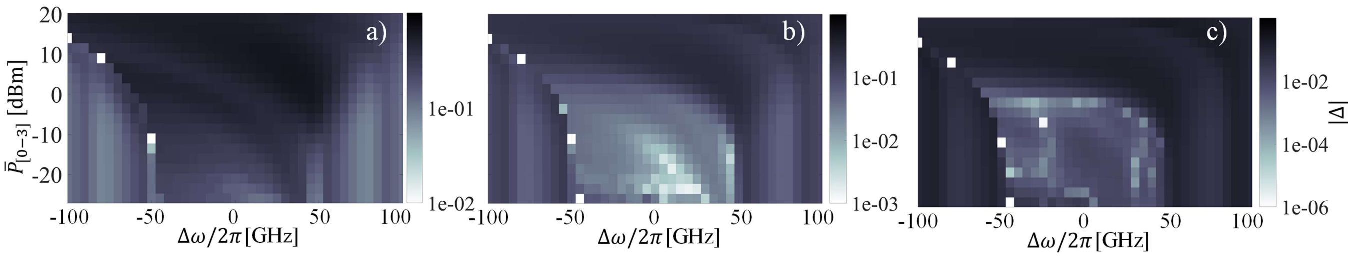

Figure S2. Difference in NMSE between: a) Channels 0 and 1, b) Channels 0 and 2, c) Channels 0 and 3, as a function of $\overline{P}_{\mathrm{i}}$ and $\Delta\omega_i/2\pi$ when addressing four different instances of the NARMA-10 task in parallel.

2 MULTIPLE OPTICAL CHANNELS ADDRESSING DIFFERENT TASKS IN PARALLEL

In this section, the system computes simultaneously four different tasks. We present the comparison between the best performance obtained for each task and previous work in the literature on photonic TDRC. This comparison includes our initial study of the proposed scheme (Giron Castro et al., 2024), in which $M = 3$. The results of each task are presented as follows: NARMA-10 in Table S1, signal waveform classification (SWC) in Table S2, wireless channel equalization (Ch.Eq) in Table S3, and the radar task in Table S4. A training set consisting of 20000 data points and 10 different testing subsets of 10000 data points were used. There is a decrease in performance with respect to previous works and $M = 3$ in the case of the wireless channel equalization task. Despite this, the system still performs with very good performance. The system appears to struggle in the case of prediction of signals that have been severely distorted as in the Ch.Eq and radar tasks. However, we also noticed such behavior on these tasks in (Giron Castro et al., 2024a) for a single optical channel scenario. Means to improve the performance per task are discussed in the main text. It is also important to notice the difference in terms of processing speed and N of this system with some of the previous implementations.

Performance: NMSE	Reference
0.168 ± 0.015, N = 50 at 0.2 GBd	(Paquot et al., 2012) (Exp., ST)
0.107 ± 0.012, N = 50 at 0.9 MBd	(Vinckier et al., 2015) (Exp., ST)
0.062 ± 0.008, N = 50 at 0.9 MBd	(Vinckier et al., 2015) (Num., ST)
0.010 ± 0.009, N= 100 at 1.0 GBd	(Donati et al., 2022) (Num., ST)
0.103 ± 0.018, N = 50 at 0.4 GBd	(Chen et al., 2019) (Num., ST)
0.0151 ± 0.0021, N = 50 at 1.0 GBd	(Giron Castro et al., 2024b) (Num., ST)
0.0373 ± 0.0021, N = 50 at 1.0 GBd, $M = 3$	(Giron Castro et al., 2024) (Num., MT)
0.0271 ± 0.0014, N = 50 at 1.0 GBd, $M = 4$	This work (Num., MT)

Table S1. Performance comparison for the NARMA-10 task. ST: Single task. MT: Multiple tasks (M=4). Exp: Experimental work. Num: Numerical work.

Performance: Accuracy	Reference
$\approx 100\%$, N = 50 at 0.2 GBd	(Paquot et al., 2012) (Exp., ST)
99.75% , N = 36 at 1.0 GBd	(Vandoorne et al., 2008) (Num., ST)
99.98% , N = 50 at 1.0 GBd	(Giron Castro et al., 2024a) (Num., ST)
99.1% , N = 50 at 1.0 GBd, $M = 3$	(Giron Castro et al., 2024) (Num., MT)
99.93% , N = 50 at 1.0 GBd, $M = 4$	This work (Num., MT)

Table S2. Performance comparison for the SC task.

Performance: SER	Reference
1.3×10^{-4}, N = 50 at 0.2 GBd	(Paquot et al., 2012) (Exp., ST)
2.0×10^{-5}, N = 50 at 0.9 MBd	(Vinckier et al., 2015) (Exp., ST)
7.0×10^{-4}, N = 50 at 0.4 GBd	(Chen et al., 2019) (Num., ST)
4.0×10^{-5}, N = 50 at 0.8 GBd	(Yue et al., 2019) (Num., ST)
1.0×10^{-3}, N = 50 at 1.0 GBd	(Giron Castro et al., 2024a) (Num., ST)
7.0×10^{-4}, N = 50 at 1.0 GBd, M = 3	(Giron Castro et al., 2024) (Num., MT)
3.9×10^{-3}, N = 50 at 1.0 GBd, M = 4	This work (Num., MT)

Table S3. Performance comparison for the wireless channel equalization task at a SNR = 32 dB.

Performance: NMSE	Reference
$\approx 0.05 \pm 0.04$, N = 50 at 0.2 GBd	(Paquot et al., 2012) (Exp., ST)
$\approx 0.05 \pm 0.008$ N = 50 at 0.13 MBd	(Duport et al., 2012) (Exp., ST)
0.093, N = 50 at 1.0 GBd	(Giron Castro et al., 2024a) (Num., ST)
0.1827, N = 50 at 1.0 GBd	This work (Num., MT)

Table S4. Performance comparison for the radar task when k =2 .

REFERENCES

Chen, Y., Yi, L., Ke, J., Yang, Z., Yang, Y., Huang, L., et al. (2019). Reservoir computing system with double optoelectronic feedback loops. *Opt. Express* 27, 27431–27440. doi:10.1364/OE.27.027431

Donati, G., Mirasso, C. R., Mancinelli, M., Pavesi, L., and Argyris, A. (2022). Microring resonators with external optical feedback for time delay reservoir computing. *Opt. Express* 30, 522–537. doi:10.1364/OE.444063

Duport, F., Schneider, B., Smerieri, A., Haelterman, M., and Massar, S. (2012). All-optical reservoir computing. *Opt. Express* 20, 22783–22795. doi:10.1364/OE.20.022783

Giron Castro, B. J., Peucheret, C., and Da Ros, F. (2024a). Memory capacity analysis of time-delay reservoir computing based on silicon microring resonator nonlinearities. In *SPIE Europe 2024: Machine Learning in Photonics*, eds. F. Ferranti, M. K. Hedayati, and A. Fratalocchi. International Society for Optics and Photonics (SPIE), vol. 13017, 130170R. doi:10.1117/12.3016750

Giron Castro, B. J., Peucheret, C., Zibar, D., and Da Ros, F. (2024b). Effects of cavity nonlinearities and linear losses on silicon microring-based reservoir computing. *Opt. Express* 32, 2039–2057. doi:10.1364/OE.509437

Giron Castro, B. J., Peucheret, C., Zibar, D., and Da Ros, F. (2024). Multi-task wavelength-multiplexed reservoir computing using a silicon microring resonator. *2024 International Joint Conference on Neural Networks (IJCNN)* , 1–7.doi:10.1109/IJCNN60899.2024.10650854

Paquot, Y., Duport, F., Smerieri, A., Dambre, J., Schrauwen, B., Haelterman, M., et al. (2012). Optoelectronic reservoir computing. *Sci. Rep.* 2, 287. doi:10.1038/srep00287

Vandoorne, K., Dierckx, W., Schrauwen, B., Verstraeten, D., Baets, R., Bienstman, P., et al. (2008). Toward optical signal processing using photonic reservoir computing. *Opt. Express* 16, 11182–11192. doi:10.1364/OE.16.011182

Vinckier, Q., Duport, F., Smerieri, A., Vandoorne, K., Bienstman, P., Haelterman, M., et al. (2015). High-performance photonic reservoir computer based on a coherently driven passive cavity. *Optica* 2, 438–446. doi:10.1364/OPTICA.2.000438

Yue, D., Wu, Z., Hou, Y., Cui, B., Jin, Y., Dai, M., et al. (2019). Performance optimization research of reservoir computing system based on an optical feedback semiconductor laser under electrical information injection. *Opt. Express* 27, 19931–19939. doi:10.1364/OE.27.019931